Time-evolution growth of Ag nanolayers on differently-passivated Si(001) surfaces

J. K. Bal and S. Hazra*

Surface Physics Division, Saha Institute of Nuclear Physics, 1/AF Bidhannagar, Kolkata 700064, India
(Received 7 January 2009; revised manuscript received 12 March 2009; published 6 April 2009)

The growth and evolution of Ag nanolayers on differently-passivated Si(001) substrates at ambient condition have been studied. Initial compactness and smoothness of Ag nanolayer on the H-passivated Si(001) surface are found better compared to those on the Br-passivated Si(001) surface, which can be understood considering surface free energy and surface mobility of the passivated surfaces. As the time passes, the growth of dewetted three-dimensional (3D) islandlike structures (Volmer-Weber-type mode) from comparatively wetted Ag nanolayer (Stranski-Krastanov-type mode) is evident at ambient conditions. Such evolution of growth is through dewetting (related to the change in the interfacial energy due to the oxide growth), migration, and coalesce of Ag, which can even produce large epitaxial [Ag(001)/Si(001)] 3D islands on H-passivated Si(001) surface. The growth rate, size, number density, and epitaxy/nonepitaxy of 3D islands are different for different passivated surfaces. These differences can be realized considering the growth time of oxide (i.e., instability of passivated surface), in-plane inhomogeneity of interfacial energy (i.e., inhomogeneous nature of passivation), and in-plane diffusion of Ag on the passivated surfaces.

I. INTRODUCTION

Ag (compared to Al and Cu) has been recognized as a potential interconnection material for ultralarge-scale integration (ULSI) technology because of its high electrical conductivity and high electromigration resistance. As the dimensions of electronic devices decrease with increasing packing density, the thickness of metal layers decreases continuously. Accordingly, understanding of the growth of metal thin film on a semiconductor becomes important both from fundamental and practical points of view.[1] In general, there are three known thin-film growth modes: layer-by-layer [Frank–van der Merwe (FM)], island [Volmer-Weber (VW)], and layer-plus-island [Stranski-Krastanov (SK)] growth modes.[2,3] Which growth mode will be adopted by a given system will depend on the surface free-energy terms and on the lattice mismatch. A great deal of effort has been devoted in controlling and/or altering the film growth using foreign species or "surfactants."[4] Introduction of a foreign atomic layer (of hydrogen, bromine, etc.) in place of clean or oxide layer on substrate surface[5–14] can change its surface energy and/or roughness, which can alter the growth mode and morphology of an overlayer. The morphology and structure of that thin overlayer plays significant role in its electrical[15] and other physical properties.

The effects of deposition conditions on the morphology of thin Ag films on Si have been investigated extensively in recent decades. Ag is found to grow epitaxially on both Si(001) and Si(111) through coincident site lattice matching, though there is a large (25%) lattice mismatch.[16–20] Epitaxial Ag films have been obtained mostly by molecular-beam epitaxy (MBE) process, where the energy of depositing particles is relatively low. While using magnetron sputtering process, Ag films usually obtained are nonepitaxial with ⟨111⟩ as the preferred growth orientation.[21,22] However, in few works, epitaxial growth of Ag on native oxide-covered Si(100) has been observed by magnetron sputtering process at higher temperatures.[23,24] Epitaxial growth of Ag on H-passivated and Br-passivated Si(111) substrates has been observed above room temperature (RT).[25–31] But there is no such report of epitaxial growth of Ag on H-Si(001) at RT.

It is clear from the large number of studies of Ag films on Si that Ag dewets the native oxide-covered Si (OSi) surface[32,33] and wets the clean Si surface.[5] If γ_m and γ_s are the surface free energies of metal and substrate, respectively, and γ_{in} is the metal-substrate interface free energy, then Ag on OSi needs to satisfy dewetting condition: $\gamma_m + \gamma_{in} > \gamma_s$ and Ag on clean Si needs to satisfy wetting condition: $\gamma_m + \gamma_{in} < \gamma_s$.[3] These can be well understood by considering the surface energies ($\gamma_m \sim 1.1 - 1.2$ J/m^2 for Ag, $\gamma_s \sim 1.2$ J/m^2 for clean Si, and $\gamma_s \sim 0.3 - 0.6$ J/m^2 for OSi) (Refs. 34–36) and simply neglecting the interfacial energies. Although Ag on clean Si satisfies wetting condition, it is not necessary that it always form epitaxial film. Studies suggest that epitaxy can be achieved either by slow deposition (such as MBE) or by enhanced surface migration. Enhanced surface migration or in-plane diffusion can be achieved by raising the growth temperature[23,24] or by introducing foreign atoms.[5,12] Better epitaxial film has been obtained on H-passivated Si surface, which has been attributed to enhanced surface migration and increased nucleation site density. In general, it is accepted that by passivating the surface differently, one can grow thin films of different morphology and epitaxy. It is also known that this passivation is not stable for longer time in open air, even in the presence of overlayer (such as Au).[37] With time, passivated layer desorbs[9] and native oxide layer grows at the metal-semiconductor interface,[37] which can change the surface and interface energies, leading to a modification in the film growth. No study has been made so far to monitor such later stages of growth of Ag on Si, which is very important from the stability point of view and gives rise to the possibility of studying interesting growth transition. Understanding of physical phenomena associated with stability and growth transition will be useful for getting required structures by controlling the growth.

In this paper, using complementary techniques, we have monitored both in-plane and out-of-plane evolutions of Ag

nanolayers deposited on differently-passivated Si(001) substrates. It has been observed that the interfacial instability *at ambient conditions* induces the wetting to dewetting transition in the Ag nanolayers, which then provides interesting nanostructures having different size, number density, and even crystallinity and/or epitaxy, depending on initial Si(001) surface passivation conditions. An attempt has been made to understand such transition considering change in interfacial energies.

II. EXPERIMENT

For the present work we have deposited thin Ag film of thickness of about 11 nm on *n*-type Si(001) of resistivity $5-10$ Ω cm using a dc magnetron sputtering unit (PLS 500, Pfeiffer) for 2 min. The substrates were sonicated by trichloro-ethelene (10 min) and methyl alcohol (10 min) separately to remove organic contaminations. Then one set was etched by hydrofluoric acid (HF) (10%) after sonication to remove the native oxide layer, so it is likely to be passivated by hydrogen whereas the second set was Br passivated (thoroughly rinsed by 0.05% Br-methanol solution) after the removal of the oxide layer by HF etching. These substrates were loaded into the sputtering chamber for Ag deposition. The power and the argon pressure were maintained at 25 W and 3.2×10^{-3} mbar, respectively, in the chamber during the deposition. Ag-deposited films on these three types of pretreated substrates were designated as Ag-OSi(001), Ag-HSi(001), and Ag-BrSi(001), respectively.

X-ray reflectivity (XRR) measurements of Ag nanolayers on differently pretreated Si(001) substrates were carried out using a versatile x-ray diffractometer (VXRD) (D8 Discover, Bruker AXS) setup.[37] VXRD consists of a diffractometer with Cu source (sealed tube) followed by a Göbel mirror to select and enhance Cu $K\alpha$ radiation (λ=1.54 Å). The diffractometer has a two-circle goniometer $[\theta - 2\theta]$ with quarter-circle Eulerian cradle as sample stage. The latter has two circular (χ and ϕ) and three translational (X, Y, and Z) motions. Scattered beam was detected using NaI scintillation (point) detector. Data were taken in specular condition, i.e., the incident angle (θ) is equal to the reflected angle (θ), and both are in the same scattering plane. Under such condition, a nonvanishing wave-vector component, q_z, is given by $(4\pi/\lambda)\sin\theta$ with resolution of 0.0014 Å^{-1}. XRR technique[38,39] essentially provides an electron-density profile (EDP), i.e., in-plane ($x-y$) average electron density (ρ) as a function of depth (z) in high resolution.[32,37] To see the evolution of EDP, XRR data for one set of samples were collected as a function of time after keeping that set at ambient conditions, while for other set of samples, XRR data have been collected just before and after the samples were in ultrahigh vacuum (UHV) conditions. X-ray diffraction (XRD) data around Ag(111) and Ag(002) peaks were collected as a function of time for the same set of samples that kept at ambient conditions for monitoring the evolution of crystallinity and/or epitaxy. Prior to XRR measurements, x-ray beam was aligned parallel to the Si(004) plane. Also to find out the major crystalline directions of Ag(111) and Ag(002) planes, rocking scans across those peaks were performed.
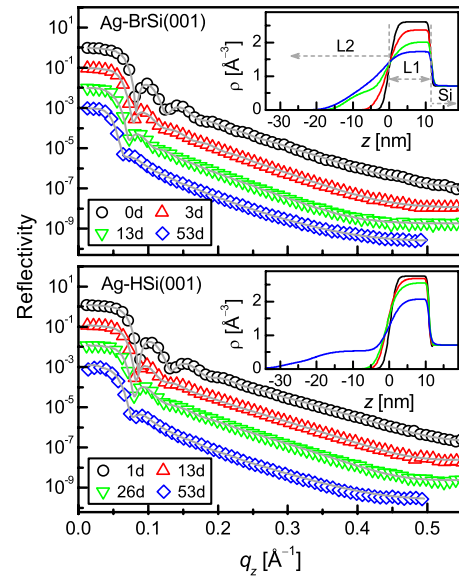

FIG. 1. (Color online) Time-evolution XRR data (different symbols) and analyzed curves (solid line) of Ag nanolayers on two differently pretreated Si(001) substrates at ambient conditions in two panels. In each panel, data and curves are shifted vertically for clarity. In legends, "d" indicates the time in day. Inset: corresponding analyzed EDPs, which consist of two layers (L1 and L2) above the Si substrate as indicated.

The topography of the Ag nanolayers on differently-passivated Si(001) substrates in small scales but in great details was mapped through atomic force microscopy (AFM) technique (Nano Scope IV, Veeco or AutoProbe CP, PSI) at ambient conditions and also mapped through scanning tunneling microscopy (STM) technique (beam-deflection AFM, Omicron NanoTechnology) at UHV condition ($\sim 10^{-10}$ mbar) to separate out the effect of ambient conditions on the evolution of sample topography. WSXM software[40] has been used for processing and analysis of both AFM and STM images. The evolution of topography in large area and in greater statistics of the Ag nanolayers on differently-passivated Si(001) substrates at ambient conditions was mapped through scanning electron microscopy (SEM) technique (Quanta 200, FEG).

III. RESULTS AND DISCUSSION

A. Growth and evolution at ambient condition

1. Electron-density profile and its evolution

Time-evolution XRR data of Ag nanolayers on differently-passivated Si(001) substrates at ambient conditions are shown in Fig. 1. Oscillations are evident in all curves, which shift toward the lower q_z value with time. The shift, however, depends strongly on the initial passivation conditions. Very rapid shift is observed in the XRR profile of the Ag-BrSi(001) sample compared to the Ag-HSi(001) sample. There is no significant change in the XRR profiles for the Ag-OSi(001) sample (not shown here) and excluded from further discussion. To obtain the quantitative information (such as EDP), XRR profiles of these samples have been
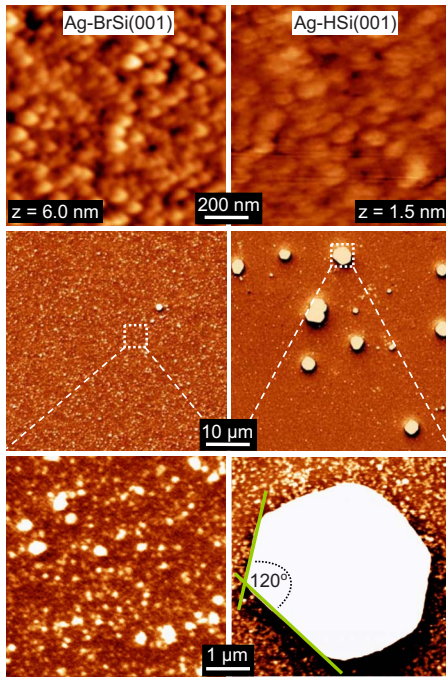
FIG. 2. (Color online) Topography of Ag nanolayers on two differently pretreated Si(001) substrates in two columns. Top panel: AFM images showing initial topography. z indicates maximum height variation. Middle and bottom panels: SEM images in two length scales showing time-evolution topography at ambient conditions. Well-faceted planes and angle between them are indicated for the dewetted Ag island on the H-passivated Si(001) surface.

analyzed using the formalism of Parratt.[41] For the analysis, each sample has been divided into a number of layers with roughness at each interface.[32,37] The EDPs obtained from the fitting of the data are shown in the inset of Fig. 1. It can be noted that all EDPs can be divided into three parts: first part is the Si substrate of constant electron density; second part is L1, the original deposited Ag layer (of fixed thickness about 11 nm) at the bottom, the electron density of which decreases with time, and third part is L2, the top Ag layer that forms due to migration of Ag from original layer, both thickness and electron density of which increase with time. However, the initial values of different parameters and their variation with time are different for different samples. The peak value of ρ of the L1 layer for the Ag-BrSi(001) sample changes from 2.6 to $1.8e/\text{Å}^3$, whereas that for the Ag-HSi(001) sample changes from 2.75 to $2e/\text{Å}^3$.

2. Topography and its evolution

Typical AFM images of Ag nanolayers, taken just after deposition on different passivated Si(001) substrates, are shown in Fig. 2. Initial topography, obtained from the AFM images, suggests that all films are composed of islands. However, the height variation in the Ag-BrSi(001) sample is large compared to that of the Ag-HSi(001) sample. Correspondingly, compactness of the latter nanolayer is more, which is also consistent with the EDP. This indicates that the wetting of Ag nanolayer on the HSi(001) substrate is comparatively better, while dewetting of the Ag nanolayer on the
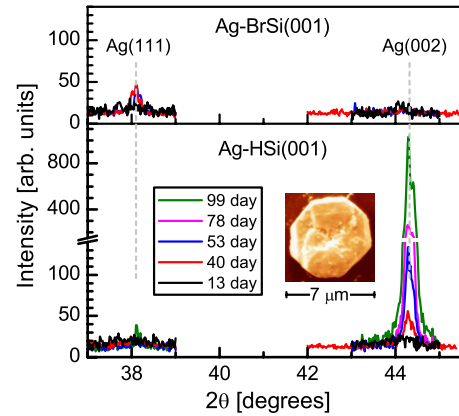

FIG. 3. (Color online) Time-evolution XRD data (around two Bragg peaks as indicated) of Ag nanolayers on two differently pretreated Si(001) substrates at ambient conditions in two panels. Inset: SEM image showing typical island structure of Ag that evolved with time on the H-passivated Si(001) surface.

BrSi(001) substrate starts even in the initial stage. It is necessary to mention that the formation of nearly dewetted structure of Ag nanolayer on the OSi(001) substrate (not shown here) is observed. The evolution of topography, monitored using SEM images, is shown in Fig. 2. Growth of large size islands with time is clearly evident. The large size islands that grow in the Ag-BrSi(001) sample have large number density and size distribution having size less than 1 μm. On the other hand, for the Ag-HSi(001) sample, number density and size distribution of large size islands are found to be small, having size in the range of 1–8 μm. The shapes of the islands on the latter sample show faceting nature similar to that observed for directed crystalline or epitaxial growth. It is necessary to mention that such three-dimensional (3D) islands in the Ag-HSi(001) sample do not present in the initial stages, which we have verified by taking AFM images in different portions of the film. From the SEM images it may appear that the top of the 3D islands for the Ag-HSi(001) sample is very smooth, which is not the case. Due to the focusing on the two-dimensional (2D) layer, it cannot be resolved beyond a certain height, and accordingly we see bright white islands. However, when we focus mainly on the top of the 3D islands, we found that the surface (shown later) is not smooth at all. This makes them very difficult to image using AFM. Other portions of the samples where 3D islands are not present have been imaged quite well using AFM, which shows an increase in roughness compared to the initial stages, consistent with the decrease in material (electron density) on that portion.

3. Toward crystallinity and/or epitaxy

Crystalline or epitaxial nature of the samples at ambient conditions has been verified monitoring time-evolution XRD data, mainly Ag(111) and Ag(002) Bragg peaks, as shown in Fig. 3. For the Ag-BrSi(001) sample, the intensity of the Ag(002) peak is almost negligible, while the intensity of the Ag(111) peak increases slightly with time. On the other hand, for the Ag-HSi(001) sample, the intensity of the Ag(002) peak increases appreciably with time, while the in-
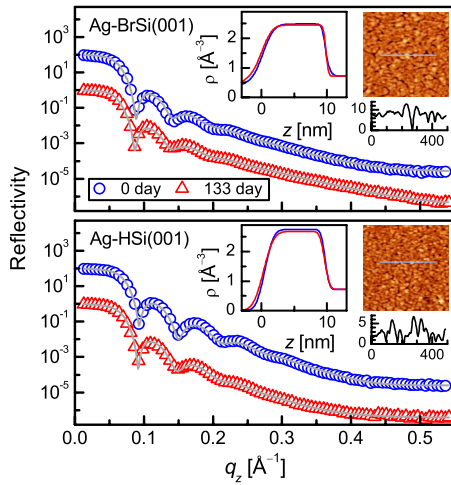
FIG. 4. (Color online) Time-evolution XRR data (different symbols) and analyzed curves (solid line) of Ag nanolayers on two differently pretreated Si(001) substrates at UHV conditions in two panels. In each panel, data and curves are shifted vertically for clarity. Inset: corresponding analyzed EDPs and STM image (of scan size 750×750 nm^2) along with line profile showing height variation (in nm).

tensity of the Ag(111) peak remains almost negligible. It can be noted that the Ag(111) peak is the 100% peak of the bulk crystal structure and expected to be observed[21,22] even if films are composed of randomly oriented Ag nanocrystals. The fact that no Ag(111) peak has been observed in the initial stages may be related to the low thickness (about 11 nm) of the film. The intensity of different peaks becomes observable with time as 3D islands grow from more thin 2D structures (as evident from EDP and topography). The slight increase in the Ag(111) peak intensity having no preferred direction (as confirmed from rocking curve) for the Ag-BrSi(001) sample is a clear signature of nontextured growth of 3D islands of Ag on the BrSi(001) surface. On the other hand, appreciable increase in the Ag(002) peak intensity having preferred direction ($\langle 001 \rangle$ direction of Si substrate as obtained from rocking curve) for the Ag-HSi(001) sample suggests epitaxial [Ag(001)/Si(001)] growth of 3D islands of Ag on the HSi(001) surface with time.

B. Growth and evolution at UHV condition

Time-evolution XRR data of Ag thin films on differently-passivated Si(001) substrates at UHV conditions are shown in Fig. 4. EDPs obtained from the analysis of XRR data are shown in the inset of Fig. 4. It can be noted from the XRR profiles that there are almost no changes in the samples with time as long as those are at UHV conditions, which is also evident from the corresponding EDPs. STM images of the same samples (when at UHV conditions) collected at different time suggest that there is no appreciable change in the topography of the samples with time. Typical topography of each samples along with a line profile are shown in the inset of Fig. 4. Height variation in the Ag-BrSi(001) sample is found to be greater compared to that of the Ag-HSi(001) sample, consistent with the EDPs, suggesting initial small
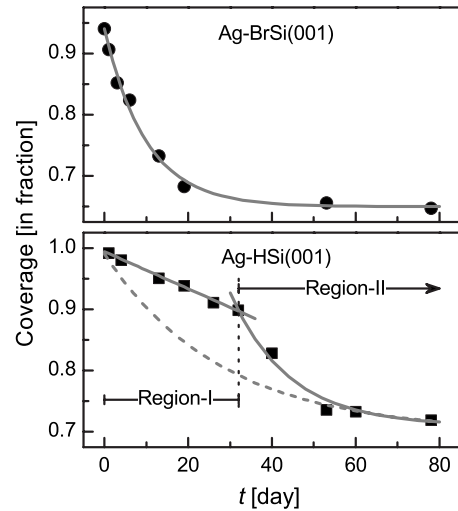

FIG. 5. Variation in coverage of Ag (from original L1 layer) with time on two differently pretreated Si(001) substrates at ambient conditions in two panels. In the top panel, solid line represents simple exponential decay. In the bottom panel, two regions exist (separated by dotted line). Solid line in region I corresponds to linear decay, while solid line in region II corresponds to exponential decay. Dashed line indicates possible exponential decay considering the whole range.

dewetting nature of the Ag-BrSi(001) sample and better wetting nature of the Ag-HSi(001) sample, which, however, remain unchanged with time in UHV conditions.

C. Dewetting and epitaxy: A controlled evolution

In order to understand the evolution of the Ag nanolayer at ambient conditions, the variation in its coverage on different passivated surfaces is plotted as a function of time in Fig. 5. The coverage (C in fraction) of the nanolayer is calculated from the EDP by considering the peak value of ρ at L1 layer in a particular time, normalized with the corresponding bulk value ($2.77e/\text{Å}^3$). It is evident from Fig. 5 that the nature of the variation in C for two samples is very much different. For the Ag-BrSi(001) sample, coverage decays very rapidly from the beginning in exponential nature, while for the Ag-HSi(001) sample, two different types of decay (classified in two regions) have been observed. In region I, i.e., up to about 32 days, the decay of coverage is very slow and linear in fashion, while in region II, i.e., beyond 32 days, the decay of coverage is similar in nature to that of the Ag-BrSi(001) sample.

The variation in coverage can be quantitatively analyzed using the following general relations:

$$C(t) = \begin{cases} 1 - \frac{1 - C_c}{t_c} t & \text{for } t \le t_c \\ (C_c - C_\infty)e^{-(t - t_c)/\tau} + C_\infty & \text{for } t \ge t_c, \end{cases} \quad (1)$$

where t_c is the critical time (for transition from linear to exponential nature), C_c is the corresponding value of the coverage, C_∞ is the final coverage, and τ is the decay time. Analysis of the time-evolution coverage data using Eq. (1) is shown in Fig. 5. Parameters obtained from the analysis are

$t_c \approx 0$ day, $C_c \approx 0.94$, $C_\infty \approx 0.65$, and $\tau \approx 10$ days for the Ag-BrSi(001) sample; while $t_c \approx 32$ days, $C_c \approx 0.9$, $C_\infty \approx 0.7$, and $\tau \approx 14$ days for the Ag-HSi(001) sample. Considering slow linear decays in region I, the value of τ for the latter sample is quite large. This can also be realized (from $\tau \approx 28$ days) if we analyze the whole range of data with exponential function (dashed curve in Fig. 5) for comparison.

The decay of Ag coverage can be related to the growth of oxide layer on the passivated Si(001) surface, which takes place even in the presence of metal layer.[37] However, the oxide growth in the Ag-Si(001) system is very slow compared to that in the Au-Si(001) system[37] and covers only about 30% of the surface area. It is known that the Ag/Si interface is less reactive compared to the Au/Si interface,[42] which makes the former interface abrupt and probably slow down the diffusion of oxygen at the interface through Ag layer. The dewetting that occurs with time produces 3D islands, which are different in crystalline nature for different samples, as evident from the XRD data (Fig. 3). For the Ag-BrSi(001) sample, even though the evolution is fast, no appreciable change in the Ag(111) or Ag(002) Bragg-peak intensity has been observed, suggesting that 3D islands are not epitaxial. On the other hand, for the Ag-HSi(001) sample, even though the evolution is slow, appreciable change in the Ag(002) Bragg-peak intensity at the later stages of evolution has been observed, suggesting epitaxial growth of 3D islands.

It is known that surface and interface free energies govern the growth mode of metal thin film on semiconductor surface,[3,43] and any change in these energies (namely, γ_s and γ_{in} due to the oxide growth) with time can strongly alter the growth mode of the film (from wetted to dewetted nature) on the substrates. The surface energy of H-passivated Si(001) surface (γ_{HSi}) is known,[36] which is less than that of the clean Si(001) surface (γ_{Si}) but comparable to that of the oxide-covered Si(001) surface (γ_{OSi}). On the other hand, the surface energy of Br-passivated Si(001) surface (γ_{BrSi}) is not known. If we consider it to be comparable with that of the H-passivated Si(001) surface, then evolution of dewetted structures on both Br- and H-passivated Si(001) surfaces are mainly related to the interfacial free energy (which includes adhesion, in-plane diffusion, etc.) and its change with time. The values of free energy and its change due to instability, which we are concerned about, are the average value. The passivated surface is not homogeneous in terms of passivation. Due to this inhomogeneity some areas (can be referred to as the strongly passivated area) of the surface remain passivated for longer time compared to others (can be referred to as the weakly passivated area) when exposed to open air, even in the presence of overlayer (Ag, Au). For the weakly passivated areas, fast desorption of H or Br atoms followed by the growth of oxide layer takes place, while for the strongly passivated areas, oxide layer rarely grows as the desorption is slow or almost negligible. The number density and size of dewetted structures, which we observed here, are related to this inhomogeneous nature of the passivated surface, while the value of τ is related to the average instability of the passivated surface, which is different for different surface passivation.

Variation in initial growth or wetability of Ag nanolayer on different passivated surface, which is mainly related to the initial interfacial free energy, suggests that $\gamma_{Ag-HSi} \lessgtr \gamma_{Ag-BrSi} < \gamma_{Ag-OSi}$. The value of γ_{Ag-HSi} or $\gamma_{Ag-BrSi}$, however, changes with time and tries to be the value of γ_{Ag-OSi}. This means that if the initial energy difference is greater ($\gamma_{Ag-OSi} - \gamma_{Ag-HSi} > \gamma_{Ag-OSi} - \gamma_{Ag-BrSi}$) then it takes more time ($\tau_{Ag-HSi} > \tau_{Ag-BrSi}$) to become γ_{Ag-OSi}, making the evolution or dewetting slow. Within the surface, dewetting (after deposition) starts from the weakly passivated areas, where the fast growth of the native oxide layer quickly changes the interfacial free energies. Accordingly, Ag atoms on weakly passivated areas leave 2D layer (L1) and go on top of the remaining L1 layer. It can be noted that the origin of the observed dewetting on passivated surface with time at ambient condition here is quite different from the surface unwetting during growth on clean surface at UHV condition found earlier.[43] The number density and size of dewetted structures evolved in the Ag-BrSi(001) sample indicate that the BrSi(001) surface has large number of strongly Br-passivated areas, which are very small in size. Growth of 3D structures having no preferred crystallographic direction takes place around those strongly passivated points by dewetting from weakly passivated area. However, dewetted Ag atoms cannot diffuse easily over relatively rough L1 layer, which restrict the size of 3D islands. It is known that large mobility of Ag on the H-passivated Si(001) surface can help to form better wetted as well as epitaxial layer, which is evident in the Ag-HSi(001) sample. The high compactness and epitaxial nature of the Ag film probably control the initial slow linear growth of dewetted structures at ambient conditions, while the high exponential growth time of dewetted Ag structures is related to the high stability of the HSi(001) surface compared to that of the BrSi(001) surface.[37] The growth of small number density and relatively large size of Ag structure with time indicate that the HSi(001) surface has small number of strongly H-passivated areas, which are relatively large in size. Growth of large 3D epitaxial structures takes place around those strongly passivated area by dewetting from weakly passivated area and large in-plane diffusion through smooth L1 layer over strongly H-passivated area. Well-faceted layered structures within large 3D islands are evident form the SEM image (shown in the inset of Fig. 3), which seem to form due to migration and coalesce of small islands.[44,45]

IV. CONCLUSIONS

The growth process of Ag nanolayers on differently-passivated Si(001) substrates and its time evolution at ambient conditions have been investigated using complementary techniques such as XRR, XRD, AFM, and SEM. SK (layer-plus-island)-type growth mode of Ag nanolayers have been observed initially, which is more toward the FM (layer-by-layer)-type growth mode on the H-passivated Si(001) surface, while that on the Br-passivated Si(001) surface is more toward the VW (island)-type growth mode as observed on the native oxide-covered Si(001) surface. Such initial growth modes remain almost unchanged in UHV conditions, while at ambient conditions strong evolution of growth has been observed. Dewetted 3D islandlike structures evolved due to the oxide growth at the interface. On the Br-passivated

Si(001) surface, fast growth of large number of small size 3D structures having no preferential crystallographic direction has been observed, while on the H-passivated Si(001) surface, slow growth of small number of large size well-faceted 3D epitaxial [Ag(001)/Si(001)] structures has been observed. Such transition from relatively wetted to dewetted structures of the Ag nanolayer having epitaxy or not, along with initial growth, can be understood considering interfacial energies as $\gamma_{Ag-HSi} \ll \gamma_{Ag-BrSi} < \gamma_{Ag-OSi}$. Surface free energy, surface mo-bility, and surface instability of the passivated surfaces govern and control the growth and evolution of such interesting structures of silver on silicon.

*satyajit.hazra@saha.ac.in

[1] B. Gergen, H. Nienhaus, W. H. Weinberg, and E. W. McFarland, Science **294**, 2521 (2001).

[2] I. Daruka and A.-L. Barabási, Phys. Rev. Lett. **79**, 3708 (1997).

[3] V. A. Shchukin and D. Bimberg, Rev. Mod. Phys. **71**, 1125 (1999).

[4] M. Copel, M. C. Reuter, E. Kaxiras, and R. M. Tromp, Phys. Rev. Lett. **63**, 632 (1989).

[5] K. Sumitomo, T. Kobayashi, F. Shoji, K. Oura, and I. Katayama, Phys. Rev. Lett. **66**, 1193 (1991).

[6] W. Widdra, S. I. Yi, R. Maboudian, G. A. D. Briggs, and W. H. Weinberg, Phys. Rev. Lett. **74**, 2074 (1995).

[7] A. Nishiyama, G. ter Horst, P. M. Zagwijn, G. N. van der Hoven, J. W. M. Frenken, F. Garten, A. R. Schlatmann, and J. Vrijmo-eth, Surf. Sci. **350**, 229 (1996).

[8] T. Yasue and T. Koshikawa, Surf. Sci. **377-379**, 923 (1997).

[9] L. Huang, S. J. Chey, and J. H. Weaver, Phys. Rev. Lett. **80**, 4095 (1998).

[10] B. Sundaravel, A. K. Das, S. K. Ghose, K. Sekar, and B. N. Dev, Appl. Surf. Sci. **137**, 11 (1999).

[11] M. Sakurai, C. Thirstrup, and M. Aono, Phys. Rev. B **62**, 16167 (2000).

[12] T. Muller and H. Nienhaus, J. Appl. Phys. **93**, 924 (2003).

[13] V. Derycke, P. G. Soukiassian, F. Amy, Y. J. Chabal, M. D. D. Angelo, H. B. Enriquez, and M. G. Silly, Nature Mater. **2**, 253 (2003).

[14] L. Ma, J. Wang, Q. Lu, and G. Wang, Chem. Phys. Lett. **405**, 208 (2005).

[15] L. Gavioli, K. R. Kimberlin, M. C. Tringides, J. F. Wendelken, and Z. Zhang, Phys. Rev. Lett. **82**, 129 (1999).

[16] F. K. LeGoues, M. Liehr, M. Renier, and W. Krakow, Philos. Mag. B **57**, 179 (1988).

[17] G. A. Smith, K.-H. Park, G.-C. Wang, T.-M. Lu, and W. M. Gibson, Surf. Sci. **233**, 115 (1990).

[18] D. C. McKenna, G.-C. Wang, and K. Rajan, J. Electron. Mater. **20**, 753 (1991).

[19] T. C. Nason, L. You, and T.-M. Lu, J. Appl. Phys. **72**, 466 (1992).

[20] K. Takahiro, S. Nagata, and S. Yamaguchi, Appl. Phys. Lett. **69**, 2828 (1996).

[21] S. Tanaka, T. Abe, and T. Yamashina, Chem. Lett. **3**, 599 (1974).

[22] N. Marechal, E. Quensnel, and Y. Panleau, J. Vac. Sci. Technol. A **12**, 707 (1994).

[23] J. H. Je, T. S. Kang, and D. Y. Noh, J. Appl. Phys. **81**, 6716 (1997).

[24] T.-B. Hur, H. K. Kim, and J. Blachere, Phys. Rev. B **75**, 205306 (2007).

[25] R. Naik, C. Kota, B. U. M. Rao, and G. W. Auner, J. Vac. Sci. Technol. A **12**, 1832 (1994).

[26] X. B. Zhang, R. L. Yasiliev, G. Van Tendeloo, Y. He, L.-M. Yu, and P. A. Thiry, Surf. Sci. **340**, 317 (1995).

[27] K. Fukutani, H. Iwai, Y. Murata, and H. Yamashita, Phys. Rev. B **59**, 13020 (1999).

[28] K. Oura, V. G. Lifshits, A. A. Saranin, A. V. Zotov, and M. Katayama, Surf. Sci. Rep. **35**, 1 (1999).

[29] I. Matsuda, H. W. Yeom, K. Tanikawa, K. Tono, T. Nagao, S. Hasegawa, and T. Ohta, Phys. Rev. B **63**, 125325 (2001).

[30] T. Fujino, T. Okuno, M. Katayama, and K. Oura, Jpn. J. Appl. Phys., Part 2 **40**, L1173 (2001).

[31] A. Arranz, J. F. Sanchez-Royo, J. Avila, V. Perez-Dieste, P. Du-mas, and M. C. Asensio, Phys. Rev. B **65**, 075405 (2002).

[32] S. Kundu, S. Hazra, S. Banerjee, M. K. Sanyal, S. K. Mandal, S. Chaudhuri, and A. K. Pal, J. Phys. D **31**, L73 (1998).

[33] S. Banerjee, S. Mukherjee, and S. Kundu, J. Phys. D **34**, L87 (2001).

[34] T. Castro, R. Reifenberger, E. Choi, and R. P. Andres, Phys. Rev. B **42**, 8548 (1990).

[35] C. T. Campbell, Surf. Sci. Rep. **27**, 1 (1997).

[36] S. Mathew, B. Satpati, B. Joseph, and B. N. Dev, Appl. Surf. Sci. **249**, 31 (2005).

[37] J. K. Bal and S. Hazra, Phys. Rev. B **75**, 205411 (2007).

[38] I. K. Robinson and D. J. Tweet, Rep. Prog. Phys. **55**, 599 (1992).

[39] *X-Ray and Neutron Reflectivity: Principles and Applications*, ed-ited by J. Daillant and A. Gibaud (Springer, Paris, 1999).

[40] I. Horcas, R. Fernandez, J. M. Gomez-Rodriguez, J. Colchero, J. Gomez-Herrero, and A. M. Baro, Rev. Sci. Instrum. **78**, 013705 (2007).

[41] L. G. Parratt, Phys. Rev. **95**, 359 (1954).

[42] A. Cros and P. Muret, Mater. Sci. Rep. **8**, 271 (1992).

[43] J. C. Glueckstein, M. M. R. Evans, and J. Nogami, Phys. Rev. B **54**, R11066 (1996).

[44] J. M. Zuo and B. Q. Li, Phys. Rev. Lett. **88**, 255502 (2002).

[45] J. S. Palmer, P. Swaminathan, S. Babar, and J. H. Weaver, Phys. Rev. B **77**, 195422 (2008).